Toxicology and Applied Pharmacology 477 (2023) 116676

Contents lists available at ScienceDirect

Toxicology and Applied Pharmacology

journal homepage: www.elsevier.com/locate/taap

Amiodarone but not propafenone impairs bioenergetics and autophagy of human myocardial cells

Adéla Krajčová [a], Vlasta Němcová [b], Milada Halačová [a,c], Petr Waldauf [a], Martin Balík [d], František Duška [a,*]

[a] Department of Anaesthesia and Intensive Care of The Third Faculty of Medicine and Královské Vinohrady University Hospital, OXYLAB-Laboratory for Mitochondrial Physiology, Charles University, Prague, Czech Republic
[b] Department of Biochemistry, Cell and Molecular Biology and Centre for Research on Nutrition, Metabolism and Diabetes, Third Faculty of Medicine, Charles University, Prague, Czech Republic
[c] Department of Pharmacology of The Second Medical Faculty, Charles University, Prague, Czech Republic
[d] Department of Anaesthesia and Intensive Care of The First Faculty of Medicine and General University Hospital, Charles University, Prague, Czech Republic

ARTICLE INFO

Editor: Lawrence Lash

Keywords:
Amiodarone
Propafenone
Cardiac cells
Mitochondria
Energy metabolism

ABSTRACT

Cardiac and extra-cardiac side effects of common antiarrhythmic agents might be related to drug-induced mitochondrial dysfunction. Supratherapeutic doses of amiodarone have been shown to impair mitochondria in animal studies, whilst influence of propafenone on cellular bioenergetics is unknown. We aimed to assess effects of protracted exposure to pharmacologically relevant doses of amiodarone and propafenone on cellular bioenergetics and mitochondrial biology of human and mouse cardiomyocytes. In this study, HL-1 mouse atrial cardiomyocytes and primary human cardiomyocytes derived from the ventricles of the adult heart were exposed to 2 and 7 μg/mL of either amiodarone or propafenone. After 24 h, extracellular flux analysis and confocal laser scanning microscopy were used to measure mitochondrial functions. Autophagy was assessed by western blots and live-cell imaging of lysosomes. In human cardiomyocytes, amiodarone significantly reduced mitochondrial membrane potential and ATP production, in association with an inhibition of fatty acid oxidation and impaired complex I- and II-linked respiration in the electron transport chain. Expectedly, this led to increased anaerobic glycolysis. Amiodarone increased the production of reactive oxygen species and autophagy was also markedly affected. In contrast, propafenone-exposed cardiomyocytes did not exert any impairment of cellular bioenergetics. Similar changes after amiodarone treatment were observed during identical experiments performed on HL-1 mouse cardiomyocytes, suggesting a comparable pharmacodynamics of amiodarone among mammalian species. In conclusion, amiodarone but not propafenone in near-therapeutic concentrations causes a pattern of mitochondrial dysfunction with affected autophagy and metabolic switch from oxidative metabolism to anaerobic glycolysis in human cardiomyocytes.

1. Introduction

Amiodarone and propafenone are commonly used drugs for treatment of ventricular and supraventricular arrhythmias with different mechanisms of action (Soar et al., 2019). Amiodarone is a class III antiarrhythmic drug (Freemantle et al., 2011; Miyazaki et al., 2015), which has multiple effects on myocardial depolarization and repolarization that make it a very effective antiarrhythmic drug. Its primary effect is to block the potassium channels, but it can also block sodium and calcium channels and the beta- and alpha-adrenergic receptors. It prolongs the refractory period in the atrial myocardium (Edvardsson, 1993) and can be used for a range of arrhythmias, including in patients with heart failure (Mujović et al., 2020). Its advantages come with well-known side effects, which include liver damage, thyroid dysfunction, neuropathy, bradycardia, AV block, torsades de pointes, pulmonary and ocular toxicity (Trohman et al., 2019). Amiodarone is a highly lipophilic agent with the iodinated benzofuran ring, which is believed to be responsible for mitochondrial toxicity in extracardiac tissues described in animal (Spaniol et al., 2001) and human (Bețiu et al., 2021) cell lines and may represent the mechanism of some extracardiac adverse effects (Ramachandran et al., 2018; Silva Santos et al., 2017). Yet, the effect of amiodarone on cardiac tissue has been mostly reported with

* Corresponding author at: Šrobárova 50, 10034 Prague, Czech Republic.
E-mail address: frantisek.duska@lf3.cuni.cz (F. Duška).

https://doi.org/10.1016/j.taap.2023.116676
Received 8 March 2023; Received in revised form 30 August 2023; Accepted 31 August 2023
Available online 3 September 2023

suprapharmacological doses in animal models (Karkhanis et al., 2018) and, given the lack of negative inotropism of amiodarone, may not be present in humans. To our knowledge, only two recent studies tested cardiotoxicity of amiodarone and other drugs on the cell line that was derived from the fusion of primary cells from adult human ventricular heart tissues with human fibroblasts (Ahn et al., 2022; Kim et al., 2022). In this cell line, it has been demonstrated that amiodarone in near-therapeutic doses increased production of reactive oxygen species (Ahn et al., 2022) and decreased spare respiratory capacity but other mitochondrial parameters were not significantly influenced (Kim et al., 2022).

Propafenone is a class Ic anti-arrhythmic agent (Stoschitzky et al., 2016) and a potent Na^+ channel blocker. Its major electrophysiological effect is to slow conduction in fast-response tissues (Tisdale et al., 2020). Propafenone has a favorable drug tolerance and no severe side effects (Valembois et al., 2019). However, the drug may provoke arrhythmias and worsen contractility in patients with structural heart disease and low ejection fraction (Nemati and Astaneh, 2016). Very little is known about propafenone effect on mitochondria (Zheng et al., 2017) and it can be hypothesized that propafenone-induced impairment of myocardial bioenergetic may be the underlying mechanism for these side effects (Nemati and Astaneh, 2016).

In this study, we aimed to investigate the impact of amiodarone and propafenone on mitochondrial metabolism in primary human cardiomyocytes isolated from the ventricles of the adult heart and compared with their effects on HL-1 cardiac muscle cells derived from atrium of the adult mouse heart.

2. Material and methods

2.1. Cell cultures

Primary human cardiac myocytes (HCM), isolated from the ventricles of the adult heart, were obtained from PromoCell GmbH (Heidelberg, Germany) and cultured in Myocyte Growth Medium containing 5% Fetal Calf Serum, 0.5 ng/mL Epidermal Growth Factor, 2 ng/mL Fibroblast Growth Factor and 5 μg/mL Insulin at 37 °C in a humidified atmosphere of 5% CO_2. The medium was changed every 2–3 days until cells reached 70–90% confluency.

HL-1 cardiac muscle cell line, derived from adult mouse heart, was obtained from Merck Millipore (Darmstadt, Germany) and cultured on fibronectin/gelatine coated surface in Claycomb medium supplemented with 10% Fetal Bovine Serum, 100 U/mL Penicillin/ 100 μg/mL Streptomycin, 0.1 mM Norepinephrine and 2 mM L-Glutamine (Claycomb et al., 1998). In HL-1 cell line, Claycomb medium was changed daily until cells reached full confluency.

The study protocol was reviewed and approved by Medical Ethics Committee at Královské Vinohrady University Hospital (decision number EK-VP/02/0/2022).

2.2. Treatment of cells

Cells were exposed to amiodarone or propafenone (Merck Millipore, Darmstadt, Germany) freshly prepared by dilution in dimethyl sulfoxide (DMSO). Control groups were incubated in either culture medium alone or solvent control DMSO. All the experiments were performed after 24-h exposure in triplicates or tetraplicates.

2.3. Cell viability and cytotoxicity assays

Viability assay. Cell viability was analyzed using the colorimetric MTS assay (CellTiter 96® AQueous Non-Radioactive Cell Proliferation Assay; Promega, Corp., Madison, WI, USA) according to manufacturer's instructions (Hook et al., 2013).

Cytotoxicity assays. Cellular cytotoxicity was determined using the conventional colorimetric lactate dehydrogenase release assay (CyQUANT LDH Cytotoxicity Assay; Thermo Fisher, USA) according to manufacturer's instructions (CyQUANT LDH Cytotoxicity Assay Kit Product Information Sheet (Pub.No. MAN0018500 B.0), 2023). Additionally, fluorescence microscopy was performed to image propidium iodide accumulation inside the cells with impaired membrane integrity (Cao et al., 2017). The proportion of dead cells was determined when combined with a nuclear label Hoechst 33342 to identify all cells within a field (see Fig. 1, parts g and h). Given that at high concentrations of amiodarone ($\geq$ 10 μg/mL) cells were <80% viable (see Fig. 1, parts a and d), we chosen only 2 and 7 μg/mL for further experiments. DMSO concentrations used for further experiments were not toxic (< 0.15%).

2.4. Bioenergetic profile analysis

ATP content. Intracellular ATP content was quantified using the luciferase-luciferin bioluminescence assay (ATP determination kit; Thermo Fisher, USA) according to manufacturer's instructions (ATP Determination Kit (A22066), 2023).

Extracellular Flux analysis. Extracellular Flux Analyzer (Agilent Technologies Inc., Santa Clara, CA, USA) was used to measure oxygen consumption rate (OCR) and extracellular acidification rate (ECAR) in living cells seeded on 24-well plate at 37 °C at the baseline and after a sequential addition of up to four compound (Brand and Nicholls, 2011; Ferrick et al., 2008; Gerencser et al., 2009). Prior to experiments, the cardiomyocytes were seeded on 24-well XF24 V7 cell culture plates at the density of 2.5×10^4 cells/per well overnight. Subsequently, the cells were exposed to antiarrhythmics for 24 h. After the exposure, four different assays were performed.

Global mitochondrial function indices. In this experiment, respiration in intact cells was firstly measured at the baseline. After that, oligomycin (1 μM) was added to block ATP synthase (Agilent Seahorse XF Cell Mito Stress Test Kit, 2023). Uncoupling agent carbonyl cyanide-4- (trifluoromethoxy)phenylhydrazone (FCCP; 1 μM) was then injected to determine maximal respiratory capacity. Finally, antimycin A (AA; 4 μM) was added to block complex III and determine non-mitochondrial respiration.

Respiration linked to individual complexes of electron transport chain. Prior to OCR measurement, cells were permeabilized with saponin (50 μg/mL) and subsequently supplemented with pyruvate (10 mM), malate (2.5 mM) and ADP (4 mM) in Mitochondrial Assay Solution (containing 220 mM mannitol, 70 mM sucrose, 10 mM KH_2PO_4, 5 mM $MgCl_2$, 2 mM HEPES, 1 mM EGTA and 0.2% BSA) (Krajčová et al., 2017). Firstly, complex I-linked respiration was measured as the OCR decrement after injection of rotenone (3 μM). Complex II-linked respiration was analyzed after sequential addition of succinate (10 mM) and malonate (10 mM). Complex IV-linked respiration was determined as the increment of OCR after addition of ascorbate plus TMPD (10 mM and 0.2 mM, respectively) and complex III inhibitor antimycin A (4 μM).

Fatty acid oxidation. After 22 h of exposure to antiarrhythmics, cells were starved for 2 h (with amiodarone/propafenone) in low-nutrient DMEM (containing 0.5 mM Glucose, 1.0 mM Glutamine, 0.5 mM Carnitine and 1% FBS) (Agilent Seahorse XF Palmitate-BSA FAO Substrate Quickstart Guide, 2023). After the treatment, low-nutrient medium was switched to Krebs-Henseleit Buffer and incubated for additional 45 min. Subsequently, 15 min before measurement cells were incubated in etomoxir (40 μM), a widely used inhibitor of fatty acid oxidation that irreversibly binds to carnitine palmitoyltransferase I (Eistetter and Wolf, 1986). Palmitate (100 μM) was added immediately before start of the OCR measurement. After that, sequential injection of oligomycin (1 μM), FCCP (1 μM) and antimycine A (4 μM) was used to determine ATP production and maximal respiration linked to oxidation of exogenous fatty acids.

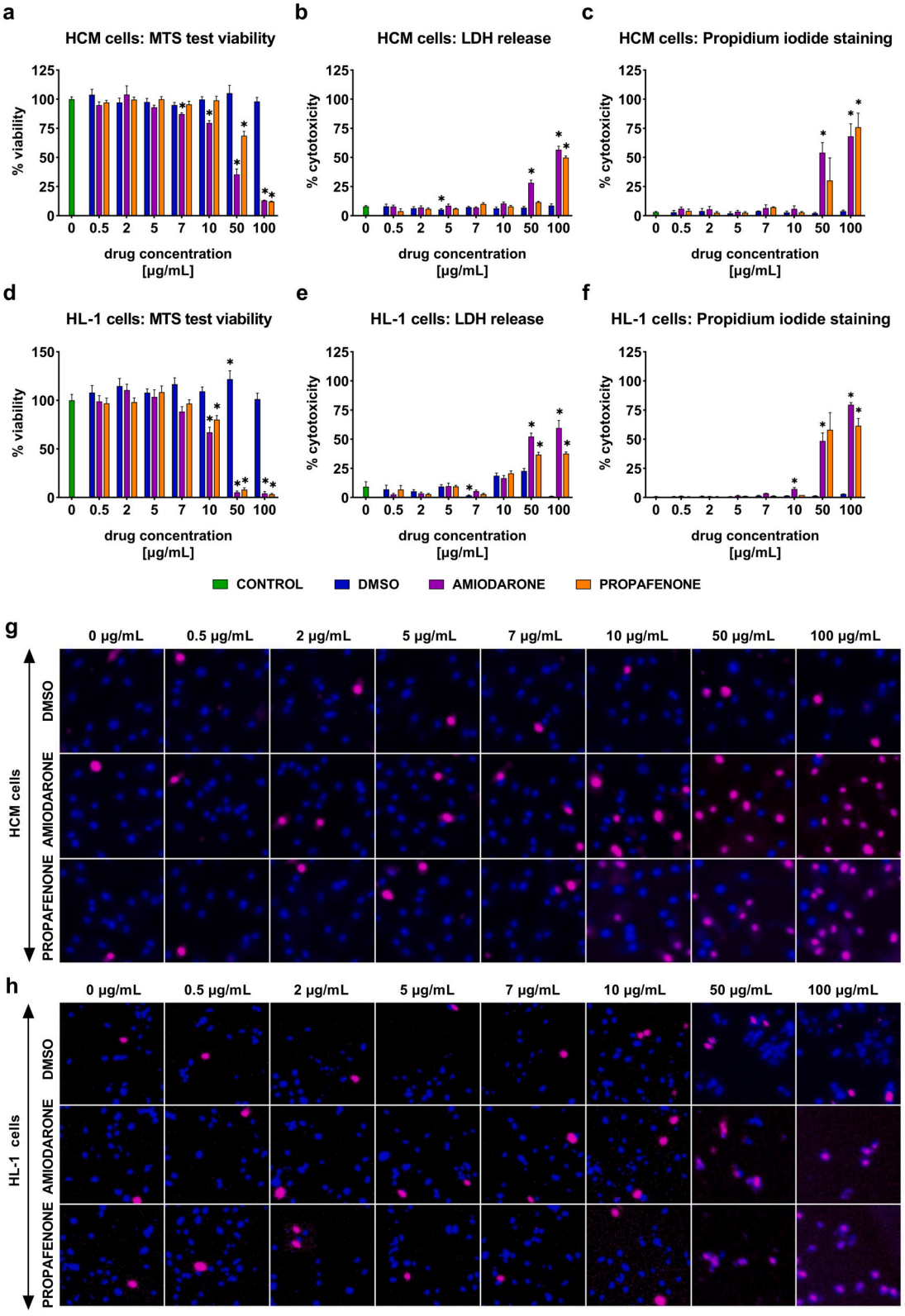

Fig. 1. Cell viability and cytotoxicity assays in primary human cardiac cells and HL-1 mouse cardiac cells. a)and **d) MTS cell viability assay in HCM cells and HL-1 cells.**Cell viability determined by MTS viability assay; **b)**and **e) LDH release in HCM cells and HL-1 cells.**% cytotoxicity calculated as the amount of lactate dehydrogenase released from dead cells with damaged plasma membrane; **c)**and **f) Propidium iodide staining in HCM cells and HL-1 cells.**% cytotoxicity expressed as the percentage of viable cells/dead cells relative to the control (= non-treated cells); **g)**and **h) Representative fluorescence microscopy images of HCM cells and HL-1 cells stained with propidium iodide.**Propidium iodide accumulated in the nuclei of dead cells with disrupted plasma membrane (purple) compared to the nuclei of viable cells with intact plasma membrane (blue). Data are presented as the mean ± SEM. Values for each group were measured in tetraplicates in 3 – 4 independent experiments. *p was considered significant at < 0.05 when compared to control group. Note: DMSO = dimethyl sulfoxide, LDH = lactate dehydrogenase, MTS = 3-(4,5-dimethylthiazol-2-yl)-5-(3-carboxymethoxyphenyl)-2-(4-sulfophenyl)-2H-tetrazolium.

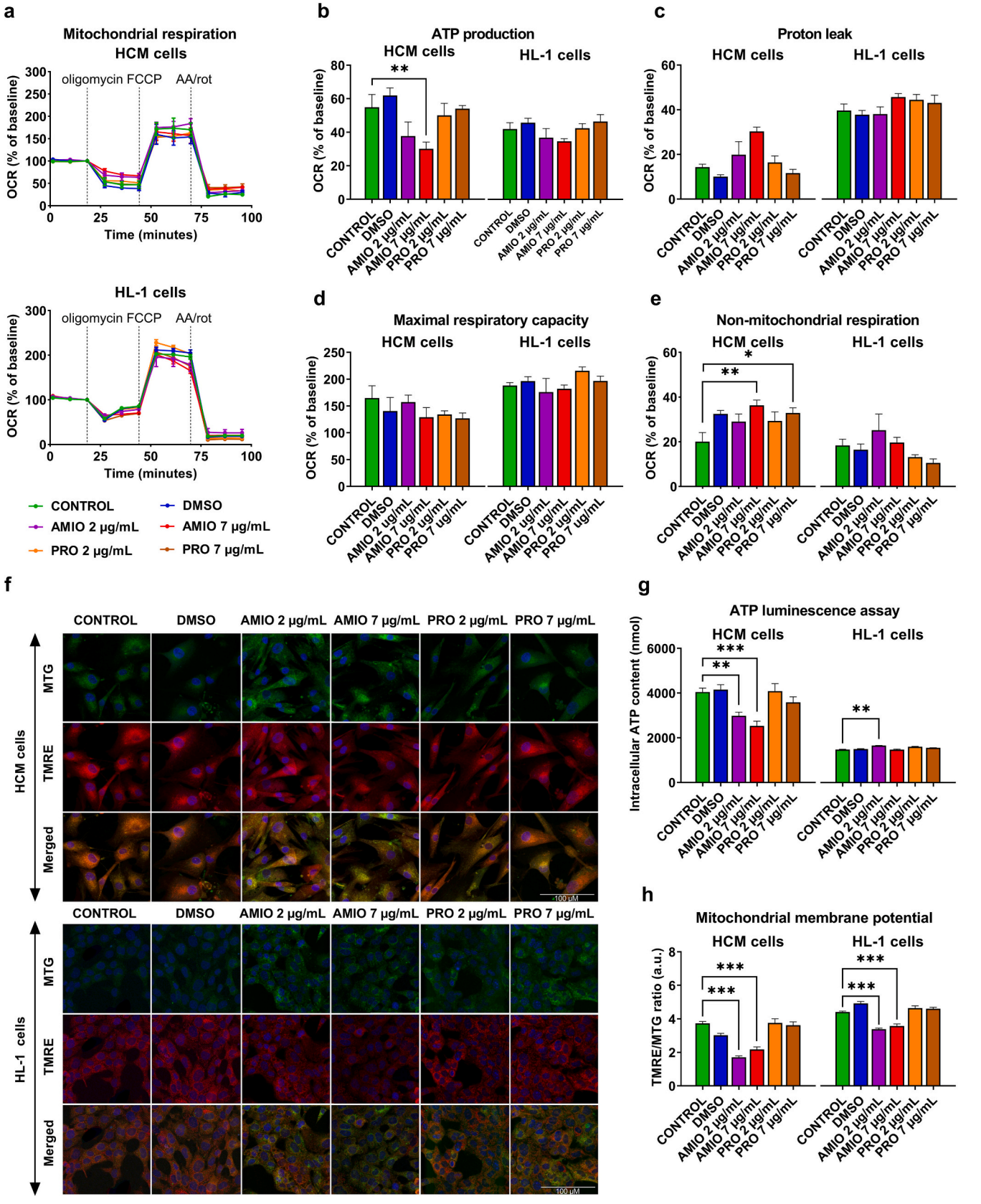

(caption on next page)

Fig. 2. Global mitochondrial parameters in primary human cardiac cells and HL-1 mouse cardiac cells. a) Real-time measurement of OCR in HCM cells and HL-1 cells at the baseline and after sequential injection of oligomycin, FCCP and antimycin A. Data are normalized to basal OCR. Each data point represents mean ± SEM from values measured in three independent experiments (n = 9-12 wells per each condition); **b) ATP production in HCM cells and HL-1 cells** calculated as the last OCR measurement before oligomycin injection minus lowest OCR measurement after oligomycin injection. Data are presented as mean ± SEM and normalized to basal OCR; **c) Proton leak in HCM cells and HL-1 cells** calculated as the lowest OCR measurement after oligomycin injection minus non-mitochondrial respiration. Data are presented as mean ± SEM and normalized to basal OCR; **d) Maximal respiratory capacity in HCM cells and HL-1 cells**calculated as highest OCR measurement after FCCP injection minus non-mitochondrial respiration. Data are presented as mean ± SEM and normalized to basal OCR; **e) Non-mitochondrial respiration in HCM cells and HL-1 cells** determined as lowest measurement of OCR after injection of rotenone and antimycin A. Data are presented as mean ± SEM and normalized to basal OCR; **f) Representative confocal images of human cardiomyocytes and HL-1 cells stained with MitoTracker™ Green FM and tetramethylrhodamine ethyl ester to detect mitochondrial membrane potential. g) Intracellular ATP content in HCM cells and HL-1 cells**measured by ATP luminescent assay. Data are presented as mean ± SEM from values measured in three independent experiments (n = 9 wells per each condition); **h) Mitochondrial membrane potential in HCM cells and HL-1 cells**calculated as the ratio of TMRE and MTG fluorescence intensity. Data are presented as mean ± SEM from values measured in four independent experiments (n ≥ 50 cells per each condition); *p < 0.05, **p < 0.01, *** p < 0.001 vs. control group. Note: OCR = oxygen consumption rate, DMSO = dimethyl sulfoxide, AMIO = amiodarone, PRO = propafenone, FCCP = carbonyl cyanide-4- (trifluoromethoxy) phenylhydrazone, AA = antimycin A, rot = rotenone, ATP = adenosine triphosphate, TMRE = tetramethylrhodamine ethyl ester, MTG = MitoTracker™ Green FM.

Glycolytic stress test. Measurement of ECAR enables to measure protons extrusion from glycolytic pathway into the medium surrounding the cells and therefore reflect glycolysis (Agilent Seahorse XF Glycolysis Stress Test Kit, 2023). Prior to ECAR measurement, the cells were pretreated in "starvation" glucose-free medium containing 2 mM glutamine for 2 h. ECAR was measured at the baseline after subsequent addition of glucose (10 mM) to determine glycolytic capacity. Oligomycin (1 μM) was then injected to block oxidative phosphorylation. Increment of ECAR allowed to measure glycolytic capacity. Finally, a glucose analog, 2-deoxy-glucose (2-DG; 50 mM) was added to inhibit glycolysis and determine non-glycolytic acidification.

All calculations of mitochondrial parameters are indicated in Fig. legends, specifically for each experiment.

2.5. Confocal laser scanning imaging

Mitochondrial membrane potential. In parallel with mitochondrial respiration analysis, membrane potential (ΔΨm) was determined and quantified in living cells using Confocal Laser Scanning Microscopy with a 63× oil immersion objective (*Leica TCS SP5* system, Leica Microsystems). After 24 h of incubation in various experimental conditions, cardiomyocytes were stained on glass coverslips with a cell permeant positively-charged red dye tetramethylrhodamine ethyl ester (TMRE; 7 nm), that readily accumulates in active mitochondria due to their relative negative charge. Prior to staining with TMRE, cells were also stained with MitoTracker™ Green FM (MTG; 200 nm) to normalize the values on mitochondrial volume(Poot et al., 1996). The fluorescence was then examined under normal growth conditions (37 °C, 5% CO_2). MitoTracker™ Green FM fluorescence was excited at 488 nm and TMRE was excited at 549 nm (Rieger et al., 2019). Mitochondrial membrane potential was calculated as a ratio of TMRE fluorescence intensity to MTG fluorescence intensity.

ROS production. After 24 h of incubation in experimental conditions, cells were loaded with MitoTracker™ Red CM-H2XRos (100 nM) to detect accumulation of mitochondrial specific-reactive oxygen species. MitoTracker Red CM-H2XRos is a reduced, non-fluorescent version of MitoTracker Red dye, that fluoresces upon oxidation (Bailey et al., 2005; Hao et al., 2006; Rieger et al., 2019). The fluorescence intensity was excited at 561 nm under normal growth conditions (37 °C, 5% CO_2).

Autophagy and lysosomal staining. After 24 h of incubation in antiarrhythmics, cardiomyocytes were loaded with LysoTracker™ Deep Red (75 nm) for 1 h to stain acidic lysosomes. After the treatment, cells were washed and incubated in live-cell imaging solution with a nuclear dye NucBlue. After additional 45 min, they were imaged under normal growth conditions (37 °C, 5% CO_2). The fluorescence of LysoTracker™ Deep Red was excited at 651 nm.

For each experiment, confocal laser scanning imaging was performed in three or four independent replicates. The numbers of cells quantified per conditions are reported in each Fig. legend.

2.6. Western blots

Samples containing 6 μg of proteins were mixed with sample buffer and denatured by heating at 45 °C for 15 min. SDS-PAGE and Western blotting were performed as described previously (Jiroutková et al., 2015). Briefly, proteins were separated on 12% polyacrylamide gels at 120 V and then blotted onto 0.2 μm nitrocellulose membrane (Protran BA83, Schleicher-Schuell, Dassel, Germany) for 3 h at 0.25 A. The membranes were blocked in 5% weight/volume bovine serum albumin in Tris-buffered saline for 30 min at room temperature. The washed membranes were probed with OxPhos Human WB Antibody Cocktail at 4 °C overnight (dilution 1:200, # 45–8199, Invitrogen), containing primary antibodies against Complex IV (F1α; 54 kDa), Complex III (core 2; 48 kDa), Complex II (29 kDa), Complex IV (COX II subunit, 22 kDa) and Complex I (18 kDa) subunits. Subsequently, we aimed to detect CPT1B as the major isoform of CPT1 expressed in the adult heart (Van Der Leij et al., 2002) and LC3B as the standard marker of autophagy (Kuma et al., 2007). For CPT1B and LC3B detection following primary antibodies were used: anti-CPT1B (dilution 1:500, ABIN2782633, Antibodies-online) and anti-LC3B (dilution 1:1000, #12741, Cell Signalling). After washing, the membranes were incubated for 2 h at room temperature with corresponding horseradish peroxidase-conjugated secondary antibody (dilution 1:10000; Proteintech). Protein bands were visualized with an enhanced chemiluminescence detection system (Thermo Fisher Scientific) using ChemiDoc™ MP Imaging System (Biorad). To demonstrate equal loading, the membrane was re-probed with anti-GAPDH antibody (dilution 1:1000, ab9485, Abcam). Densitometry was performed using the Image Lab 6.1 software (Biorad).

2.7. Statistics

First, all data were tested for normality of distribution. In case of normal distribution, we used one-way ANOVA with Dunnett post hoc test. In case of non-normally distributed data, Kruskal-Wallis with Dunn's post hoc test was used. All calculations and graphs were performed in GraphPad Prism 8.0.1 (GraphPad Software, Inc., La Jolla, CA, USA). Differences at $p < 0.05$ were considered significant. The image analysis was performed using Fiji ImageJ software.

3. Results

3.1. Cell viability and cytotoxicity

In primary human cardiac cells, both amiodarone and propafenone caused a significant dose-dependent decline of cell viability at concentrations >5 μg/mL and > 10 μg/mL, respectively (see Fig. 1, part a). Similarly, in HL-1 mouse cardiomyocytes, cell viability was decreased at the concentrations ≥10 μg/mL in both agents (see Fig. 1, part d). In both cell lines, a significant number of dead cells with damaged plasma membrane was found only at the very high concentrations of both drugs

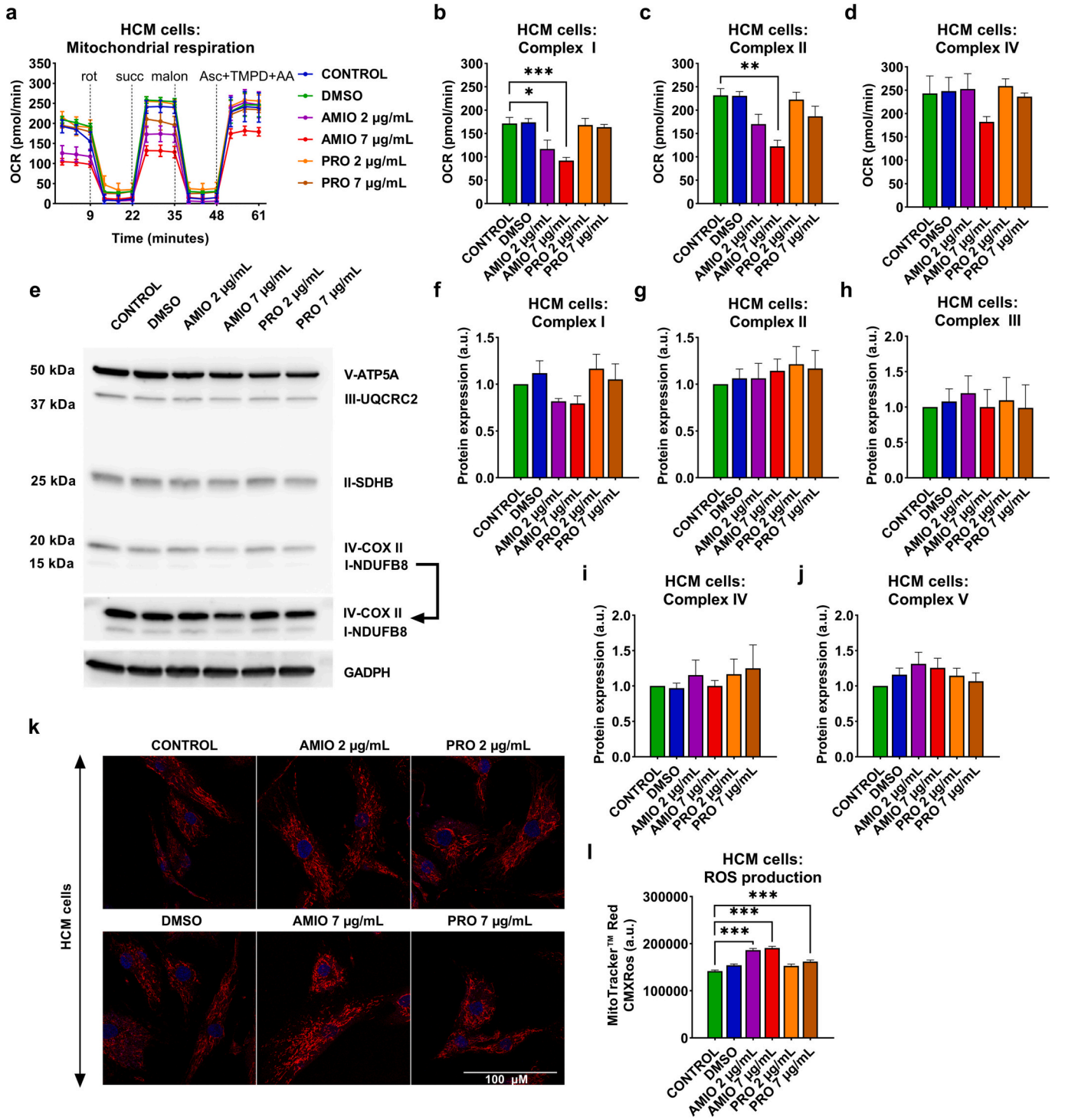

Fig. 3. Complexes of the electron transport chain and ROS production in primary human cardiac cells. a) Real-time measurement of OCR in HCM cells reflecting respiration linked to individual complexes of ECT. Each data point represents mean ± SEM from values measured in three independent experiments (n = 9-12 wells per each condition); **b) Respiration linked to complex I in HCM cells**calculated as the OCR at baseline (in the XF Assay Medium supplemented with 10 mM pyruvate, 2.5 mM malate and 4 mM ADP) minus the OCR after addition of rotenone; **c) Respiration linked to complex II in HCM cells**calculated as the OCR after succinate minus the OCR after malonate; **d) Respiration linked to complex IV in HCM cells**determined as the OCR after Ascorbate + TMPD and antimycin A; **e) Representative image of western blot of complexes of ETC in HCM cells;**Arrow shows a detail of complex I and IV (after a longer exposure for better visibility). **f) Protein expression of complex I in HCM cells.**Data are presented as mean ± SEM. **G) Protein expression of complex II in HCM cells.**Data are presented as mean ± SEM; **h) Protein expression of complex III in HCM cells.**Data are presented as mean ± SEM; **i) Protein expression of complex IV in HCM cells.**Data are presented as mean ± SEM; **j) Protein expression of complex V in HCM cells.**Data are presented as mean ± SEM; **k) Representative confocal image of HCM cells stained with MitoTracker™ Red CMXRos to detect ROS production; l) ROS production in HCM cells**determined as the fluorescence intensity of MitoTracker Red CM-H2XRos labelled cells. Data are presented as mean ± SEM from values measured in four independent experiments (n ≥ 50 cells per each condition). *p < 0.05, **p < 0.01, *** p < 0.001 vs. control group. Note: OCR = oxygen consumption rate, DMSO = dimethyl sulfoxide, AMIO = amiodarone, PRO = propafenone, rot = rotenone, succ = succinate, malon = malonate, Asc = ascorbate, TMPD = N,N,N',N'-Tetramethyl-p-phenylenediamine dihydrochloride, AA = antimycin A, GADPH = glyceraldehyde-3-phosphate dehydrogenase, ROS = reactive oxygen species.

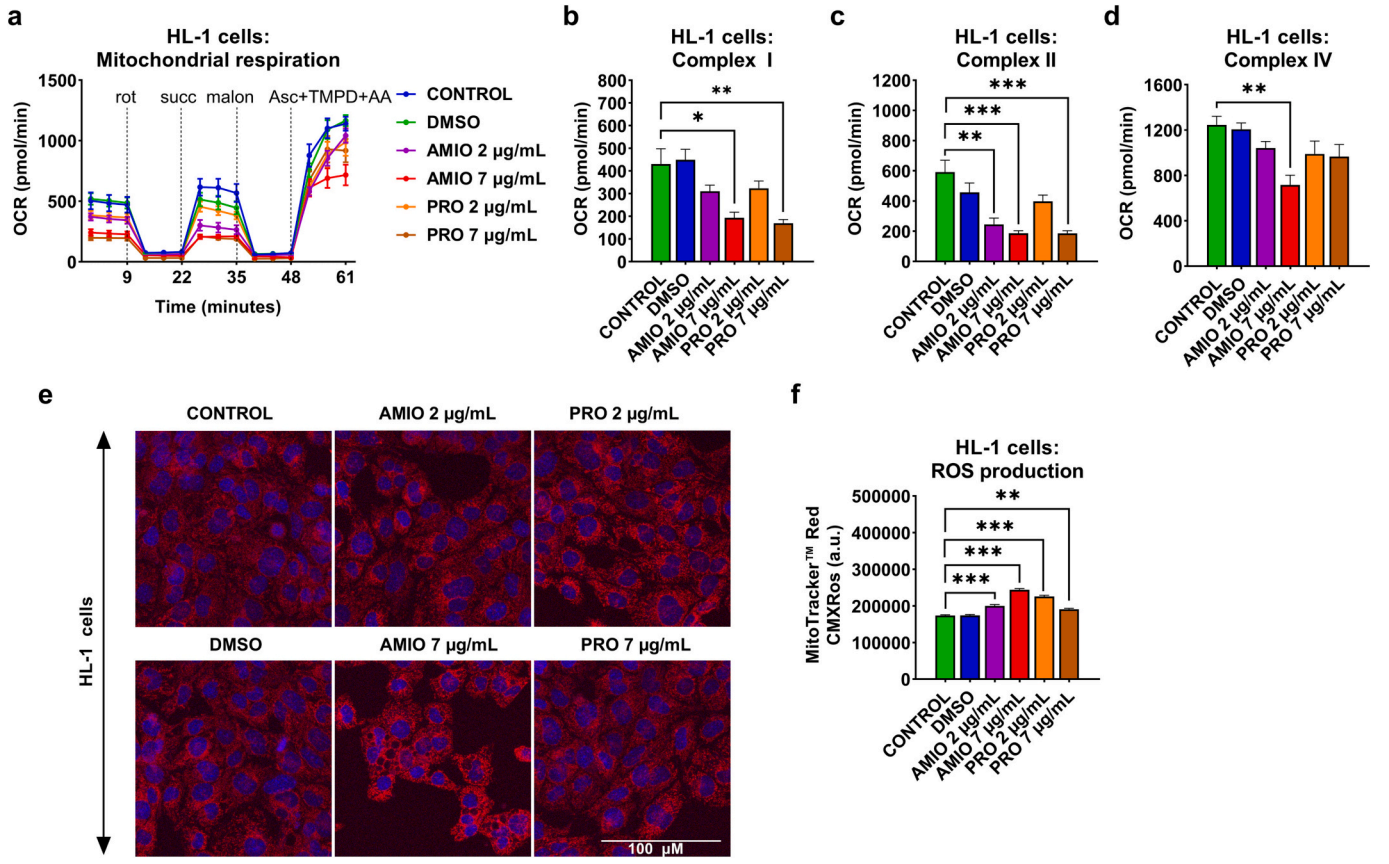

Fig. 4. Complexes of the electron transport chain and ROS production in HL-1 mouse cardiac cells. a) Real-time measurement of OCR in HL-1 cells reflecting respiration linked to individual complexes of ECT. Each data point represents mean ± SEM from values measured in three independent experiments (n = 9-12 wells per each condition); **b) Respiration linked to complex I in HL-1 cells** calculated as the OCR at baseline (in the XF Assay Medium supplemented with 10 mM pyruvate, 2.5 mM malate and 4 mM ADP) minus the OCR after addition of rotenone; **c) Respiration linked to complex II in HL-1 cells** calculated as the OCR after succinate minus the OCR after malonate; **d) Respiration linked to complex IV in HL-1 cells** determined as the OCR after Ascorbate + TMPD and antimycin A; **e) Representative confocal image of HL-1 cells stained with MitoTracker™ Red CMXRos to detect ROS production; f) ROS production in HL-1 cells** determined as the fluorescence intensity of MitoTracker Red CM-H2XRos labelled cells. Data are presented as mean ± SEM from values measured in four independent experiments (n ≥ 50 cells per each condition). *p < 0.05, **p < 0.01, *** p < 0.001 vs. control group. Note: OCR = oxygen consumption rate, DMSO = dimethyl sulfoxide, AMIO = amiodarone, PRO = propafenone, rot = rotenone, succ = succinate, malon = malonate, Asc = ascorbate, TMPD = N,N,N',N'-Tetramethyl-p-phenylenediamine dihydrochloride, AA = antimycin A, ROS = reactive oxygen species.

(≥ 50 µg/mL for amiodarone and propafenone, respectively; see Fig. 1, parts b, c, e, f, g and h). DMSO at the range of used concentrations had no significant impact on bot cell lines (see Fig. 1, parts a, b, c, d, e, f, g and h). For further experiments, we have chosen concentrations 2 and 7 µg/mL as at these concentrations ~90% of cells survive and are near the therapeutic plasma concentrations of both drugs.

3.2. Global mitochondrial functions

As demonstrated in Fig. 2, parts a and b, in primary human cardiac cells, amiodarone, but not propafenone caused significant alteration in ATP production measured as oligomycin-inhibitable O_2 consumption. In line, amiodarone but not propafenone decreased intracellular ATP content (see Fig. 2, part g) and mitochondrial membrane potential (ΔΨm; see Fig. 2, parts f and h). Proton leak tended to increase in amiodarone-exposed cells, although this did not reach statistical significance (see Fig. 2, part c). Maximal respiratory capacity was not significantly influenced among experimental groups (see Fig. 2, part d). Non-mitochondrial respiration was increased after amiodarone and propafenone treatment (see Fig. 2, part e). Given that findings in bioenergetic profile, we explored in detail possible alterations in electron transfer chain (ETC) and substrate utilization pathways.

The data from Extracellular Flux Analyzer and ATP luminescence assay obtained on HL-1 cell line showed no significant changes of global mitochondrial functions in cells exposed to neither amiodarone or propafenone (see Fig. 2, parts a, b, c, d, e and f). However, mitochondrial membrane potential was significantly decreased in amiodarone-exposed cells (see Fig. 2, parts g and h). Next, more detailed experiments confirmed changes in substrate preference in HL-1 cardiomyocytes (see Fig. 6 below) similar to those seen in human cardiomyocytes (see Fig. 5 below).

3.3. Capacity of individual ETC complexes and mitochondrial ROS production

In primary human cardiac cells, amiodarone significantly inhibited complex I and II-linked respiration in the electron transport chain (see Fig. 3, parts a, b, c and d) without altering the expression level of key subunits of these complexes (see Fig. 3, parts e, f, g, h, i and j). No significant impact was seen in neither DMSO or propafenone-exposed cells. However, both amiodarone (at the concentrations 2 and 7 µg/mL) and propafenone (at 7 µg/mL) significantly increased mitochondrial ROS production (see Fig. 3, parts k and l). In keeping with these findings, amiodarone significantly decreased complex I, II and IV-linked respiration in HL-1 mouse cardiomyocytes (see Fig. 4, parts a, b, c and d). In HL-1 cells, ROS production was significantly increased in all experimental groups compared to control groups (see Fig. 4, parts e and f).

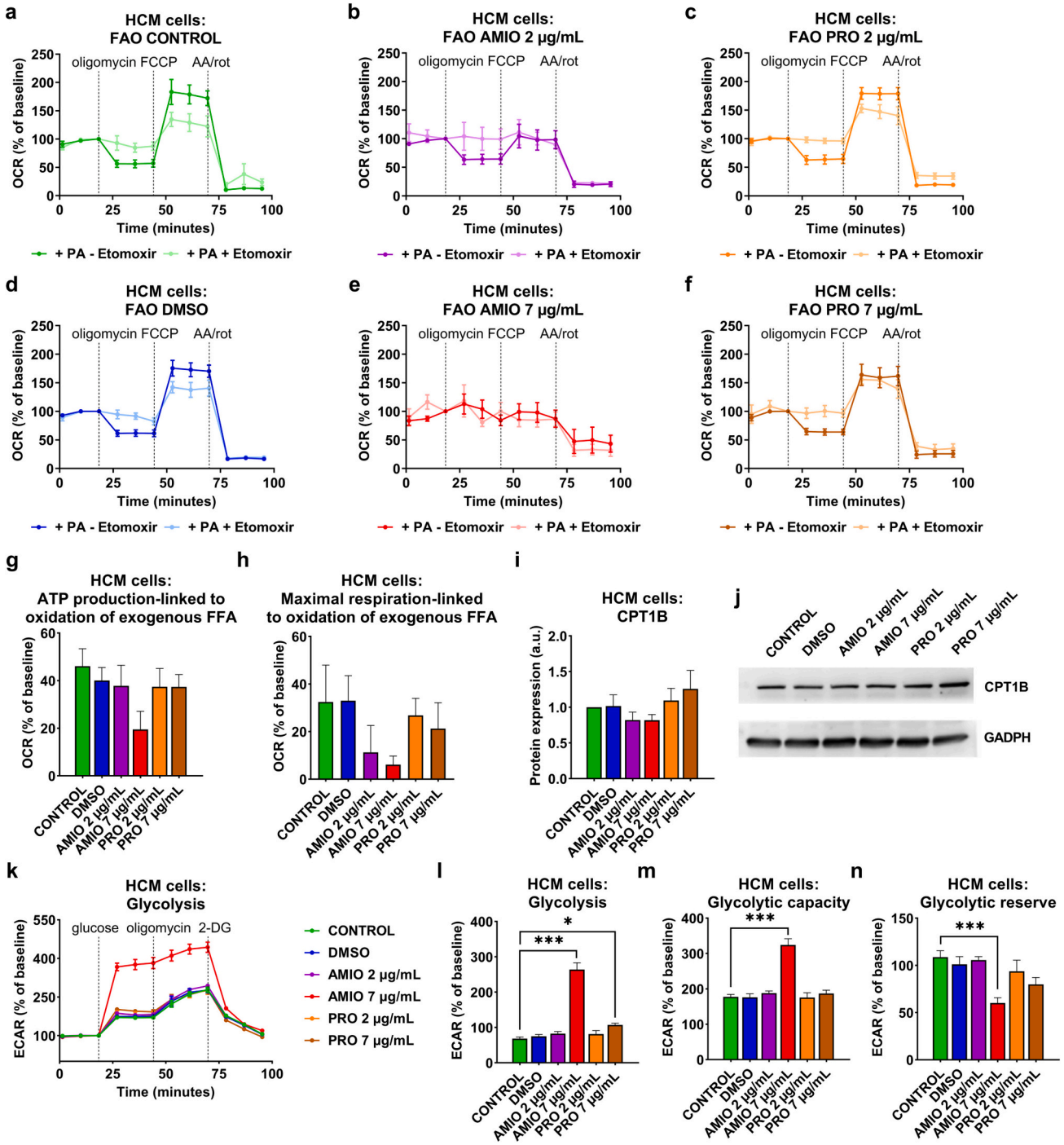

Fig. 5. Fatty acid oxidation and glycolysis pathway in primary human cardiac cells. Real-time measurement of OCR linked to oxidation of exogenous palmitate: a) in control HCM cells; b) 2 µg/mL amiodarone-exposed HCM cells; c) 2 µg/mL propafenone-exposed HCM cells; d) DMSO-exposed HCM cells; e) 7 µg/mL amiodarone-exposed HCM cells; f) 7 µg/mL propafenone-exposed HCM cells. Each data point represents mean ± SEM from values measured in four independent experiments (n = 6-12 wells per each condition); **g) ATP production linked to oxidation of exogenous palmitate in HCM cells** calculated as the last OCR measurement before oligomycin injection minus the lowest OCR measurement after oligomycin injection (only in groups not exposed to etomoxir). Data are presented as mean ± SEM and normalized to basal OCR; **h) Maximal respiration linked to oxidation of exogenous palmitate in HCM cells** calculated as the difference of the maximal OCR values after FCCP injection between groups exposed and not exposed to etomoxir. Data are presented as mean ± SEM and normalized to basal OCR; **i) Protein expression of CPT1B in HCM cells.** Data are presented as mean ± SEM; **j) Representative image of western blot of CPT1B in HCM cells; k) Real-time measurement of OCR reflecting glycolysis in HCM cells.** Each data point represents mean ± SEM from values measured in three independent experiments (n = 9-12 wells per each condition); **l) The rate of glycolysis under basal conditions in HCM cells** calculated as the maximal value of OCR after glucose injection minus non-glycolytic acidification (caused by processes in the cell other than glycolysis). Data are presented as mean ± SEM and normalized to basal OCR; **m) Maximum glycolytic capacity in HCM cells** calculated as the maximal OCR after oligomycin injection minus non-glycolytic acidification. Data are presented as mean ± SEM and normalized to basal OCR; **n) Glycolytic reserve in HCM cells** calculated as the difference between glycolytic capacity and glycolytic rate. Data are presented as mean ± SEM and normalized to basal OCR. *p < 0.05, *** p < 0.001 vs. control group. Note: OCR = oxygen consumption rate, DMSO = dimethyl sulfoxide, AMIO = amiodarone, PRO = propafenone, rot = rotenone, FAO = fatty acid oxidation, PA = palmitate, ECAR = extracellular acidification rate, CPT1B = carnitine palmitoyltransferase 1B, 2-DG = 2-Deoxy-D-glucose.

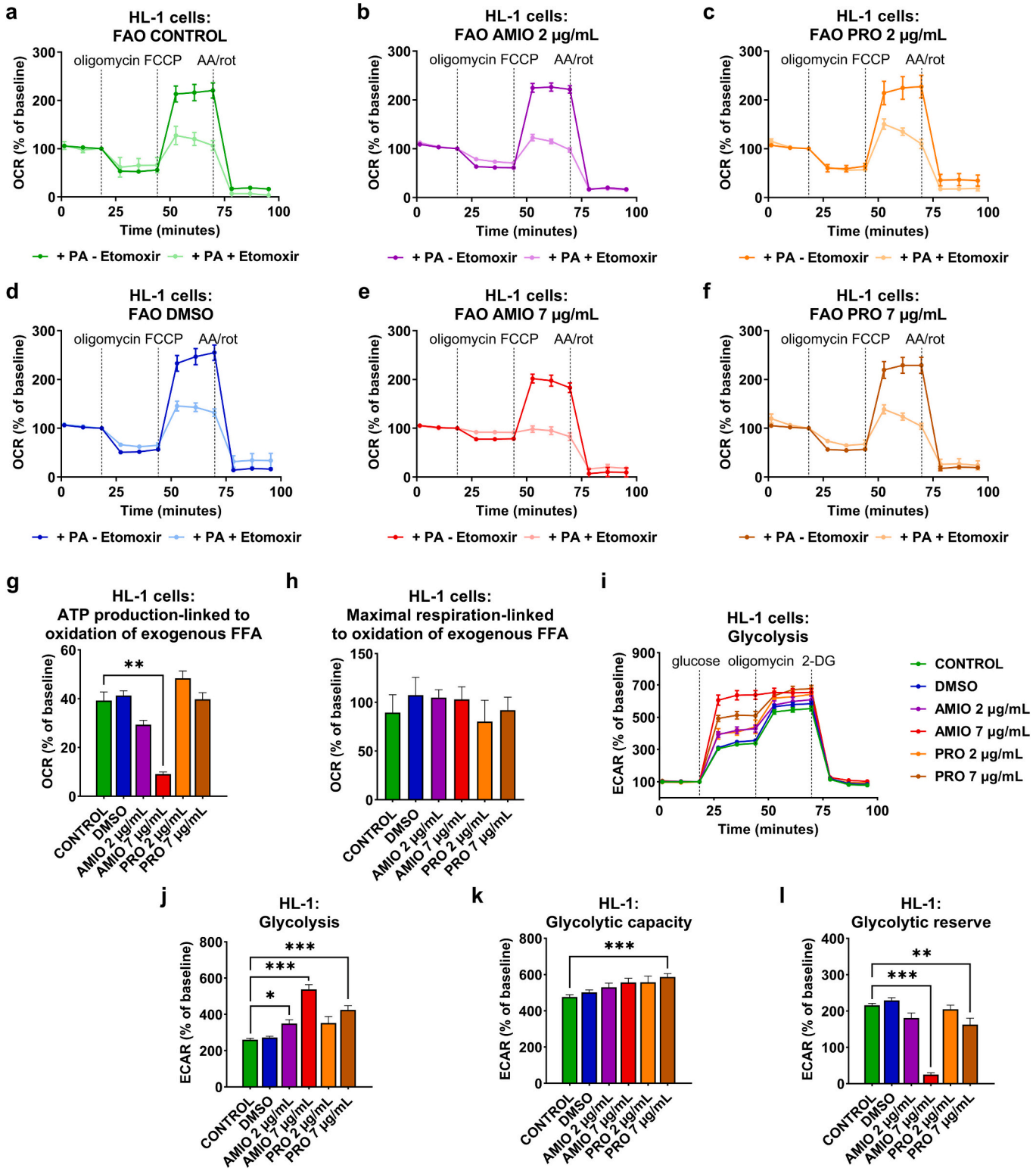

(caption on next page)

Fig. 6. Fatty acid oxidation and glycolysis pathway in HL-1 mouse cardiac cells. Real-time measurement of OCR linked to oxidation of exogenous palmitate: a) in HL-1 control cells; b) 2 μg/mL amiodarone-exposed HL-1 cells; c) 2 μg/mL propafenone-exposed HL-1 cells; d) DMSO-exposed HL-1 cells; e) 7 μg/mL amiodarone-exposed HL-1 cells; f) 7 μg/mL propafenone-exposed HL-1 cells. Each data point represents mean ± SEM from values measured in four independent experiments (n = 6-12 wells per each condition); **g) ATP production linked to oxidation of exogenous palmitate in HL-1 cells**calculated as the last OCR measurement before oligomycin injection minus the lowest OCR measurement after oligomycin injection (only in groups not exposed to etomoxir). Data are presented as mean ± SEM and normalized to basal OCR; **h) Maximal respiration linked to oxidation of exogenous palmitate in HL-1 cells**calculated as the difference of the maximal OCR values after FCCP injection between groups exposed and not exposed to etomoxir. Data are presented as mean ± SEM and normalized to basal OCR; **i) Real-time measurement of OCR reflecting glycolysis in HL-1 cells.**Each data point represents mean ± SEM from values measured in three independent experiments (n = 9-12 wells per each condition); **j) The rate of glycolysis under basal conditions in HL-1 cells**calculated as the maximal value of OCR after glucose injection minus non-glycolytic acidification (caused by processes in the cell other than glycolysis). Data are presented as mean ± SEM and normalized to basal OCR; **k) Maximum glycolytic capacity in HL-1 cells**calculated as the maximal OCR after oligomycin injection minus non-glycolytic acidification. Data are presented as mean ± SEM and normalized to basal OCR; **l) Glycolytic reserve in HL-1 cells**calculated as the difference between glycolytic capacity and glycolytic rate. Data are presented as mean ± SEM and normalized to basal OCR. *$p < 0.05$, **$p < 0.01$, *** $p < 0.001$ vs. control group. Note: OCR = oxygen consumption rate, DMSO = dimethyl sulfoxide, AMIO = amiodarone, PRO = propafenone, rot = rotenone, FAO = fatty acid oxidation, PA = palmitate, ECAR = extracellular acidification rate, 2-DG = 2-Deoxy-D-glucose.

3.4. Substrate utilization studies

In primary human cardiomyocytes exposed to 7 μg/mL amiodarone, we observed a decrease in the oxidation of fatty acids (in both ATP production and maximal respiration linked to exogenous oxidation of long-chain fatty acids; see Fig. 5, parts b, e, g and h) accompanied by increased glycolysis (see Fig. 5, parts k, l and m) compared to control groups (see Fig. 5, parts a and d) or propafenone-treated cells (see Fig. 5, parts c and f). There were no detectable changes in the expression levels of the key enzymes of these pathways (CPT1B; see Fig. 5, parts i and j), but cells exposed to higher concentration of amiodarone seemed to increase their glycolytic capacity (see Fig. 5, part m) and, correspondingly decrease the glycolytic reserve (see Fig. 5, part n). Similarly, ATP production linked to fatty acid oxidation tended to decline in amiodarone-exposed HL-1 cells (see Fig. 6, parts b, e and g), although maximal respiration was not significantly influenced (see Fig. 6, part h). In addition, HL-1 cells exposed to 7 μg/mL amiodarone exhibited enhanced glycolysis and decreased glycolytic reserve (see Fig. 6, parts i, j and l). On the contrary, fatty acid oxidation in propafenone-treated HL-1 cells did not significantly differ compared to control groups (see Fig. 6, parts a, c, d, f, g and h). However, glycolysis and glycolytic capacity was significantly increased in HL-1 cells exposed to 7 μg/mL propafenone (see Fig. 6, parts, i, j and k). Correspondingly, glycolytic reserve was decreased (see Fig. 6, part l).

3.5. Autophagy in primary human cardiac cells

After amiodarone treatment, we have observed a dose-dependent increase in the level of LC3B-II, phosphatidylethanolamine-conjugated form of LC3B protein, that is recruited into autophagosomal membranes in contrast to the unconjugated, cytosolic form (LC3B-I) and is essential for autophagosome formation. Employing LysoTracker™ Deep Red Staining, we also detected a decreased acidification in lysosomes (see Fig. 7, parts b, c, d and e). In propafenone-treated cells, we also observed a lower lysosomal acidification, despite the lack of detectable changes in LC3B-II protein expression (see Fig. 7, parts b, c, d and e). In HL-1 cells, the changes in fluorescence intensity were not so apparent, but there was a tendency to decline in both amiodarone and propafenone-exposed cells (see Fig. 7, parts b and c).

4. Discussion

In this study, we assessed changes of mitochondrial biology in both human and mouse cardiomyocytes in vitro after 24 h exposure to two widely used antiarrhythmics. Our main finding is that amiodarone, but not propafenone, causes significant dose-dependent changes of mitochondrial functions in human cardiomyocytes. We have demonstrated a complex pattern of inhibition of Complexes I and II associated with a reduction of the proton gradient across inner mitochondrial membrane and an impairment of aerobic phosphorylation, leading to a degree of metabolic switch from oxidative metabolism to anaerobic glycolysis. In addition, impaired complexes I and II increased ROS production associated with increased mitochondrial damage and autophagy. Of note, similar effects were observed with identical drug concentrations in HL-1 mouse cardiomyocytes, suggesting that the results of experiments in other mammalian species (Dzimiri and Almotrefi, 1993; Karkhanis et al., 2018; Spaniol et al., 2001) might be reproducible in human cell lines. However, at some points, HL-1 cells were found to be mildly more resistant to inhibitory effects of amiodarone than human cardiomyocytes (see ATP production and FAO in Fig. 2, parts a and b and Fig. 6, parts b, e, g and h, respectively). We therefore hypothesize that longer amiodarone exposure might be required to induce the same level of inhibition in HL-1 mouse cells.

Amiodarone is a cationic amphiphilic agent that easily crosses cell membranes and accumulates in intracellular compartments including mitochondria and lysosomes (Reinhart and Rohner, 2023; Vater et al., 2017). The accumulation occurs because in the acidic milieu of intermembrane space (pH ~ 6.8 (Bal et al., 2012)), amine moieties of amiodarone undergo protonation, which favour accumulation of amiodarone inside the negatively charged matrix (Begriche et al., 2011; Fromenty and Pessayre, 1995), where the process of protonation is reversed [pH ~ 8.0 (Bal et al., 2012)]. The transfer of amiodarone molecule may explain the observed uncoupling of the inner mitochondrial membrane, and contribute to the reduction mitochondrial membrane potential ($\Delta\Psi m$). In addition, amiodarone may alter a phospholipid content in both extracardiac tissues and heart (Rabkin, 2006) with further impairment of mitochondrial organization and function (Rosa et al., 2000; Sautereau et al., 1992). Indeed, we have observed direct inhibition of Complexes I and II of the ETC and FAO in keeping with previous studies performed on extracardiac tissues (Fromenty et al., 1990; Fromenty and Pessayre, 1995; Kennedy et al., 1996; Nicolescu et al., 2008; Pessayre et al., 2010), rabbit (Patterson et al., 1987) and guinea pig hearts (Dzimiri and Almotrefi, 1993), or rat cardiomyocytes (Kálai et al., 2005; Karkhanis et al., 2018; Kennedy et al., 1996; Nag et al., 1990; Varbiro et al., 2003) suggesting that the influence of amiodarone onto cardiac cell bioenergetics is complex, combining all the above listed mechanism.

Both antiarrhythmics increased the production of reactive oxygen species (ROS). In cardiac and other cells, damaged mitochondria are scavenged by fusing with lysosomes to autophagosomes, where the organelle is finally degraded (Yim and Mizushima, 2020) in the acidic microenvironment [pH inside lysosomes is 4.0–5.0 (Bal et al., 2012)], which is mandatory for the function of lysosomes (Zeng et al., 2020). Amiodarone has global pKa = 6.56 (Dowd, 2009), rendering its molecule completely protonated and trapped inside lysosomes (Pessayre et al., 2010). Accumulation of amiodarone increases intra-lysosomal pH, impairing lysosomal degradative function (Morissette et al., 2009). In line, in our experiments, we have seen a reduction of acidic environment in labelled lysosomes in amiodarone-exposed cells, together with increased conversion of LC3B from LC3B-I (an unconjugated form) to

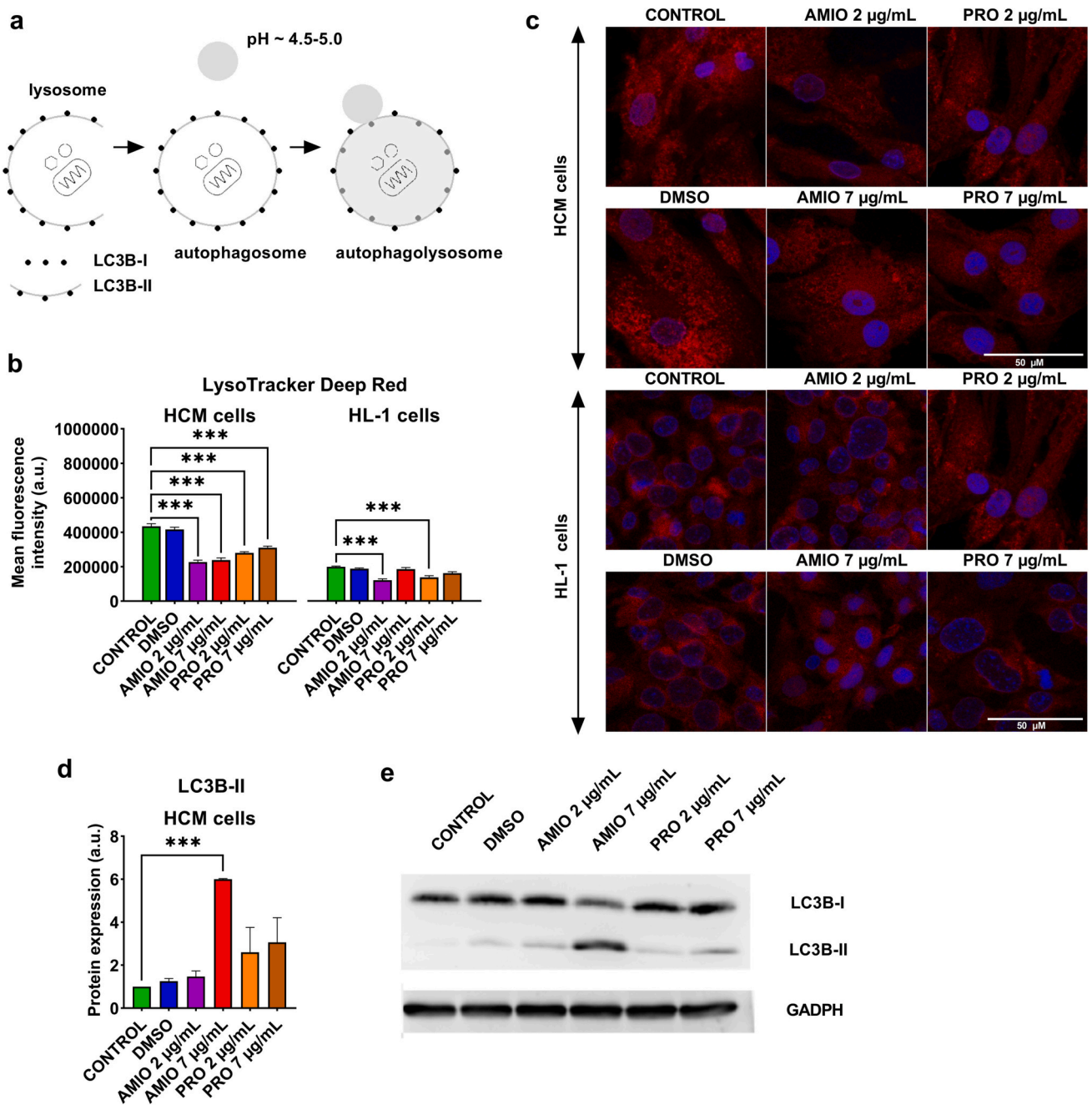

Fig. 7. Autophagy process in primary human cardiac cells and HL-1 mouse cardiac cells. a) Schematic diagram of the steps of autophagy process. An unconjugated form LC3B-I is converted to a conjugated form LC3B-II which is essential for autophagosome formation. Autophagosome formation is followed by fusion of autophagosome to acidic lysosome to form autophagolysosome. At the same time, under normal circumstances, LC3B-II is degraded in autophagolysosomal lumen and its level decreases; **b) Mean fluorescence intensity of lysosomes in HCM cells and HL-1 cells labelled with LysoTracker™ Deep Red.** Data are presented as mean ± SEM from values measured in three independent experiments (n ≥ 50 cells per each condition). **c) Representative confocal images of HCM cells and HL-1 cells stained with LysoTracker™ Deep Red to detect acidic lysosomes; d) Protein expression of LC3B-II in HCM cells.**Data are presented as mean ± SEM; **e) Representative image of western blot of autophagy marker LC3B – an unconjugated form LC3B-I and a conjugated form LC3B-II – in HCM cells;***** $p < 0.001$ vs. control group. Note: AMIO = amiodarone, DMSO = dimethyl sulfoxide, GADPH = glyceraldehyde-3-phosphate dehydrogenase, PRO = propafenone.

LC3B-II (a conjugated form) which is essential for autophagosome formation. This is consistent with the pattern of mismatch between the demand versus capacity for autophagy. It is intriguing to hypothesize that impaired autophagy might be responsible for some extracardiac side effects of amiodarone, too.

The main strength of our study is that we performed a comprehensive set of experiments in a setting as close as to human physiology as it can be in an ex vivo model. The therapeutic concentration in plasma ranges between 1.5 and 2.5 µg/mL for amiodarone (Lafuente-Lafuente et al., 2009) and between 0.20 and 0.60 µg/mL for propafenone (Steurer et al., 1991), but concentration as high as 1200 µg/mL has been seen in case of non-fatal accidental overdose (Ovaska et al., 2010). Amiodarone accumulates in tissues, reaching tissue concentrations much higher than in plasma (Latini et al., 1984). Therefore, we believe the concentrations we have chosen (2 and 7 µg/mL) well reflect the concentrations in tissues of patient treated with antiarrhythmics. This study has potential clinical

implications, too. In patients with a degree of mitochondrial dysfunction at baseline, such as in patients with sepsis, but with structurally normal heart, propafenone might be better choice (Morelli et al., 2013). The clinical outcomes consistent with this hypothesis have just been published (Balik et al., 2023).

Our results also points towards a potential for detrimental effects of amiodarone in patients with insulin resistance. This stems from the role insulin plays in regulating the heart's metabolism, primarily based on fatty acids but capable of utilizing alternatives such as carbohydrates, ketone bodies, lactate, and amino acids (Bertrand et al., 2008; Doenst et al., 2013). Insulin resistance, however, disrupts this metabolic equilibrium by reducing glucose oxidation and boosting fatty acid oxidation (Ormazabal et al., 2018). In this context, amiodarone could further restrict available energy sources, potentially affecting ATP synthesis (Pantazi et al., 2022). An energy deficit in cardiomyocytes may induce maladaptive responses, including hypertrophy, apoptosis, or fibrosis, which may have clinical consequences. In turn, propafenone might be hypothesized as a potentially safer alternative in patients with insulin resistance. These findings require further investigation.

Indeed, our study has limitations. We have only studied the parental substance, but not drug metabolites, which can be both active and toxic. For example, desethylamiodarone, preserves the benzofuran structure and hence lipophilicity, has a potential for mitochondrial toxicity (Bolt et al., 2001). On the same note, in our experiments we used chemical uncoupling and not contraction to increase ATP demands. In addition, we have not revealed the mechanism of direct inhibition of key proteins of bioenergetic pathways and some of our inferences thus remain speculative. Demands. Lastly, both amiodarone and propafenone seem to be equally safe in structurally normal hearts and performing our experiments on cellular models of heart failure (Jimenez-Tellez and Greenway, 2019; Rohani et al., 2017) could be more informative. Lastly, although propafenone has been noted to display fewer negative effects on mitochondrial function and the autophagic process compared to amiodarone in our study, this does not exclude the possibility of such effects occurring in clinical scenarios or at higher concentrations. Indeed, the overall safety profile of both antiarrhytmics is dependent on many factors and should be carefully evaluated on a case-by-case basis in clinical practice.

5. Conclusions

In conclusion, our findings from in vitro experiments on human cardiac cell lines reveal that amiodarone, but not propafenone, causes significant dose-dependent disruptions in mitochondrial bioenergetics and autophagy. These disruptions involve mitochondrial uncoupling, which impairs ATP synthesis and triggers a metabolic shift from oxidative metabolism towards anaerobic glycolysis.

Authors' contributions

A.K. was responsible for the concept and design of the study, performed the experiments, data analysis and wrote the original draft of the manuscript. V.N. performed the experiments, contributed to data analysis and edited the original draft of the manuscript. M.H. contributed to the validation and data interpretation and edited the original draft of the manuscript. P.W. performed data analysis and statistics. M.B. was responsible for funding acquisition and edited the manuscript. F.D. supervised the study, contributed to experimental planning and design, did data interpretation and discussions and contributed to the original draft of the manuscript. All authors read and approved the final manuscript.

Funding

The work has been supported from the grants of Czech Health Research Council AZV NV18–06-00417 and AZV NU21J-06-00078 and by the project National Institute for Research of Metabolic and Cardiovascular Diseases (Programme EXCELES, ID Project No. LX22NPO5104) - Funded by the European Union—Next Generation EU.

Clinical trial registration

Trial registration number NCT03029169.

Declaration of Competing Interest

The authors have no conflict of interest to declare.

Data availability

Data are available from the corresponding author upon reasonable request.

Appendix A. Supplementary data

Supplementary data to this article can be found online at https://doi.org/10.1016/j.taap.2023.116676.

References

Agilent Seahorse XF Cell Mito Stress Test Kit, 2023. WWW Document. URL Available at: https://www.agilent.com/cs/library/usermanuals/public/XF_Cell_Mito_Stress_Test_Kit_User_Guide.pdf (accessed 6.6.23).

Agilent Seahorse XF Glycolysis Stress Test Kit, 2023. WWW Document. URL Available at: https://www.agilent.com/cs/library/usermanuals/public/XF_Glycolysis_Stress_Test_Kit_User_Guide.pdf (accessed 6.6.23).

Agilent Seahorse XF Palmitate-BSA FAO Substrate Quickstart Guide, 2023. WWW Document. URL Available at: https://www.agilent.com/cs/library/usermanuals/public/XF_Palmitate_BSA_Substrate_Quickstart_Guide.pdf (accessed 6.6.23).

Ahn, D., Kim, C.W., Go, R.E., Choi, K.C., 2022. Evaluation of mitochondrial oxidative toxicity in mammalian cardiomyocytes by determining the highly reproducible and reliable increase in mitochondrial superoxides after exposure to therapeutic drugs. Toxicol. in Vitro 83. https://doi.org/10.1016/j.tiv.2022.105393.

ATP Determination Kit (A22066), 2023. WWW Document. URL Available at: https://www.thermofisher.com/document-connect/document-connect.html?url=https://assets.thermofisher.com/TFS-Assets%2FLSG%2Fmanuals%2Fmp22066.pdf (accessed 6.6.23).

Bailey, S.R., Mitra, S., Flavahan, S., Flavahan, N.A., 2005. Reactive oxygen species from smooth muscle mitochondria initiate cold-induced constriction of cutaneous arteries. Am. J. Physiol. Heart Circ. Physiol. 289, 243–250. https://doi.org/10.1152/ajpheart.01305.2004.

Bal, W., Kurowska, E., Maret, W., 2012. The final frontier of pH and the undiscovered country beyond. PLoS One 7. https://doi.org/10.1371/journal.pone.0045832.

Balik, M., Maly, M., Brozek, T., Rulisek, J., Porizka, M., Sachl, R., Otahal, M., Brestovansky, P., Svobodova, E., Flaksa, M., Stach, Z., Horejsek, J., Volny, L., Jurisinova, I., Novotny, A., Trachta, P., Kunstyr, J., Kopecky, P., Tencer, T., Pazout, J., Belohlavek, J., Duska, F., Krajcova, A., Waldauf, P., 2023. Propafenone versus amiodarone for supraventricular arrhythmias in septic shock: a randomised controlled trial. Intensive Care Med. https://doi.org/10.1007/s00134-023-07208-3.

Begriche, K., Massart, J., Robin, M.A., Borgne-Sanchez, A., Fromenty, B., 2011. Drug-induced toxicity on mitochondria and lipid metabolism: mechanistic diversity and deleterious consequences for the liver. J. Hepatol. https://doi.org/10.1016/j.jhep.2010.11.006.

Bertrand, L., Horman, S., Beauloye, C., Vanoverschelde, J.L., 2008. Insulin signalling in the heart. Cardiovasc. Res. https://doi.org/10.1093/cvr/cvn093.

Beţiu, A.M., Chamkha, I., Gustafsson, E., Meijer, E., Avram, V.F., Frostner, E.Å., Ehinger, J.K., Petrescu, L., Muntean, D.M., Elmér, E., 2021. Cell-permeable succinate rescues mitochondrial respiration in cellular models of amiodarone toxicity. Int. J. Mol. Sci. 22 https://doi.org/10.3390/ijms222111786.

Bolt, M., Card, J., Racz, W., Brien, J., Massey, T., 2001. Disruption of mitochondrial function and cellular ATP levels by amiodarone and N-desethylamiodarone in initiation of amiodarone-induced pulmonary cytotoxicity. J. Pharmacol. Exp. Ther. 298, 1280–1289.

Brand, M.D., Nicholls, D.G., 2011. Assessing mitochondrial dysfunction in cells. Biochem. J. 435, 297–312. https://doi.org/10.1042/BJ20110162.

Cao, H., Li, C., Qi, W., Meng, X., Tian, R., Qi, Y., Yang, W., Li, J., 2017. Synthesis, cytotoxicity and antitumor mechanism investigations of polyoxometalate doped silica nanospheres on breast cancer MCF-7 cells. PLoS One 12, 1–18.

Claycomb, W.C., Lanson, N.A., Stallworth, B.S., Egeland, D.B., Delcarpio, J.B., Bahinski, A., Izzo, N.J., 1998. HL-1 cells: a cardiac muscle cell line that contracts and retains phenotypic characteristics of the adult cardiomyocyte. Cell Biol. 95, 2979–2984.

CyQUANT LDH Cytotoxicity Assay Kit Product Information Sheet (Pub.No. MAN0018500 B.0), 2023.

Doenst, T., Nguyen, T., Abel, E., 2013. Cardiac Metabolism in Heart Failure - Implications beyond ATP production. Circ. Res. 113, 709–724. https://doi.org/10.1161/CIRCRESAHA.113.300376.

Dowd, F., 2009. xPharm: The Comprehensive Pharmacology Reference. Elsevier.

Dzimiri, N., Almotrefi, A.A., 1993. Actions of amiodarone on mitochondrial ATPase and lactate dehydrogenase activities in guinea pig heart preparations. Eur. J. Pharmacol. 242, 113.

Edvardsson, N., 1993. Comparison of class I and class III action in atrial fibrillation. Eur. Heart J. 14, 62–66. https://doi.org/10.1093/eurheartj/14.suppl_h.62.

Eistetter, K., Wolf, H., 1986. Etomoxir. Drugs Future 11, 1034–1036.

Ferrick, D.A., Neilson, A., Beeson, C., 2008. Advances in measuring cellular bioenergetics using extracellular flux. Drug Discov. Today 13, 268–274. https://doi.org/10.1016/j.drudis.2007.12.008.

Freemantle, N., Lafuente-Lafuente, C., Mitchell, S., Eckert, L., Reynolds, M., 2011. Mixed treatment comparison of dronedarone, amiodarone, sotalol, flecainide, and propafenone, for the management of atrial fibrillation. Europace 13, 329–345. https://doi.org/10.1093/europace/euq450.

Fromenty, B., Pessayre, D., 1995. Inhibition of mitochondrial beta-oxidation as a mechanism of hepatotoxicity. Pharmacol. Ther. 67, 101–154.

Fromenty, B., Fisch, C., Labbe, G., Degott, C., Deschamps, D., Berson, A., Letteron, P., Pessayre, D., 1990. Amiodarone inhibits the mitochondrial beta-oxidation of fatty acids and produces microvesicular steatosis of the liver in mice. J. Pharmacol. Exp. Ther. 255, 1371–1376.

Gerencser, A.A., Neilson, A., Choi, S.W., Edman, U., Yadava, N., Oh, R.J., Ferrick, D.A., Nicholls, D.G., Brand, M.D., 2009. Quantitative microplate-based respirometry with correction for oxygen diffusion. Anal. Chem. 81, 6868–6878. https://doi.org/10.1021/ac900881z.

Hao, L., Nishimura, T., Wo, H., Fernandez-Patron, C., 2006. Vascular responses to α1-adrenergic receptors in small rat mesenteric arteries depend on mitochondrial reactive oxygen species. Arterioscler. Thromb. Vasc. Biol. 26, 819–825. https://doi.org/10.1161/01.ATV.0000204344.90301.7c.

Hook, B., Bratz, M., Schagat, T., 2013. Gain more Informative Data by Multiplexing a Fluorescent Real-Time Cytotoxicity Assay with Luminescent, Fluorescent or Colorimetric Viability Assays [WWW Document].

Jimenez-Tellez, N., Greenway, S.C., 2019. Cellular models for human cardiomyopathy: what is the best option? World J. Cardiol. 11, 221–235. https://doi.org/10.4330/wjc.v11.i10.221.

Jiroutková, K., Krajčová, A., Ziak, J., Fric, M., Waldauf, P., Džupa, V., Gojda, J., Němcova-Fürstová, V., Kovář, J., Elkalaf, M., Trnka, J., Duška, F., 2015. Mitochondrial function in skeletal muscle of patients with protracted critical illness and ICU-acquired weakness. Crit. Care 19. https://doi.org/10.1186/s13054-015-1160-x.

Kálai, T., Várbiró, G., Bognár, Z., Pálfi, A., Hantó, K., Bognár, B., Osz, E., Sümegi, B., Hideg, K., 2005. Synthesis and evaluation of the permeability transition inhibitory characteristics of paramagnetic and diamagnetic amiodarone derivatives. Bioorg. Med. Chem. 13, 2629–2636. https://doi.org/10.1016/j.bmc.2005.01.028.

Karkhanis, A., Leow, J.W.H., Hagen, T., Chan, E.C.Y., 2018. Dronedarone-induced cardiac mitochondrial dysfunction and its mitigation by epoxyeicosatrienoic acids. Toxicol. Sci. 163, 79–91. https://doi.org/10.1093/toxsci/kfy011.

Kennedy, J., Unger, S., Horowitz, J., 1996. Inhibition of carnitine palmitoyltransferase-1 in rat heart and liver by perhexiline and amiodarone. Biochem. Pharmacol. 52, 273–280.

Kim, C.W., Lee, H.J., Ahn, D., Go, R.E., Choi, K.C., 2022. Establishment of a platform for measuring mitochondrial oxygen consumption rate for cardiac mitochondrial toxicity. Toxicol. Res. 38, 511–522. https://doi.org/10.1007/s43188-022-00136-2.

Krajčová, A., Løvsletten, N.G., Waldauf, P., Frič, V., Elkalaf, M., Urban, T., Anděl, M., Trnka, J., Thoresen, G.H., Duška, F., 2017. Effects of Propofol on cellular bioenergetics in human skeletal muscle cells. Crit. Care Med. 1 https://doi.org/10.1097/CCM.0000000000002875.

Kuma, A., Matsui, M., Mizushima, N., 2007. LC3, an autophagosome marker, can be incorporated into protein aggregates independent of autophagy: caution in the interpretation of LC3 localization. Autophagy 3, 323–328. https://doi.org/10.4161/auto.4012.

Lafuente-Lafuente, C., Alvarez, J.C., Leenhardt, A., Mouly, S., Extramiana, F., Caulin, C., Funck-Brentano, C., Bergmann, J.F., 2009. Amiodarone concentrations in plasma and fat tissue during chronic treatment and related toxicity. Br. J. Clin. Pharmacol. 67, 511–519. https://doi.org/10.1111/j.1365-2125.2009.03381.x.

Latini, R., Tognoni, G., Kates, R.E., 1984. Summary clinical pharmacokinetics of amiodarone. Clin. Pharmacokinet. 9, 136–156.

Miyazaki, S., Taniguchi, H., Nakamura, H., Takagi, T., Iwasawa, J., Hachiya, H., Iesaka, Y., 2015. Clinical significance of early recurrence after pulmonary vein antrum isolation in paroxysmal atrial fibrillation – insight into the mechanism. Circ. J. 79, 2353–2359. https://doi.org/10.1253/circj.CJ-15-0475.

Morelli, A., Ertmer, C., Westphal, M., Rehberg, S., Kampmeier, T., Ligges, S., Orecchioni, A., D'Egidio, A., D'Ippoliti, F., Raffone, C., Venditti, M., Guarracino, F., Girardis, M., Tritapepe, L., Pietropaoli, P., Mebazaa, A., Singer, M., 2013. Effect of heart rate control with esmolol on hemodynamic and clinical outcomes in patients with septic shock: a randomized clinical trial. JAMA 310, 1683–1691. https://doi.org/10.1001/jama.2013.278477.

Morissette, G., Ammoury, A., Rusu, D., Marguery, M.C., Lodge, R., Poubelle, P.E., Marceau, F., 2009. Intracellular sequestration of amiodarone: role of vacuolar ATPase and macroautophagic transition of the resulting vacuolar cytopathology. Br. J. Pharmacol. 157, 1531–1540. https://doi.org/10.1111/j.1476-5381.2009.00320.x.

Mujović, N., Dobrev, D., Marinković, M., Russo, V., Potpara, T.S., 2020. The role of amiodarone in contemporary management of complex cardiac arrhythmias. Pharmacol. Res. 151 https://doi.org/10.1016/j.phrs.2019.104521.

Nag, A.C., Lee, M.L., Shepard, D., 1990. Effect of amiodarone on the expression of myosin isoforms and cellular growth of cardiac muscle cells in culture. Circ. Res. 67, 51–60.

Nemati, M.H., Astaneh, B., 2016. Amiodarone versus propafenone to treat atrial fibrillation after coronary artery bypass grafting: a randomized double blind controlled trial. Korean J. Thor. Cardiovasc. Surg. 49, 177–184. https://doi.org/10.5090/kjtcs.2016.49.3.177.

Nicolescu, A.C., Ji, Y., Comeau, J.L., Hill, B.C., Takahashi, T., Brien, J.F., Racz, W.J., Massey, T.E., 2008. Direct mitochondrial dysfunction precedes reactive oxygen species production in amiodarone-induced toxicity in human peripheral lung epithelial HPL1A cells. Toxicol. Appl. Pharmacol. 227, 370–379. https://doi.org/10.1016/j.taap.2007.12.009.

Ormazabal, V., Nair, S., Elfeky, O., Aguayo, C., Salomon, C., Zuñiga, F.A., 2018. Association between insulin resistance and the development of cardiovascular disease. Cardiovasc. Diabetol. https://doi.org/10.1186/s12933-018-0762-4.

Ovaska, H., Ludman, A., Spencer, E.P., Wood, D.M., Jones, A.L., Dargan, P.I., 2010. Propafenone poisoning-a case report with plasma propafenone concentrations. J. Med. Toxicol. 6, 37–40. https://doi.org/10.1007/s13181-010-0037-2.

Pantazi, K., Karlafti, E., Bekiaridou, A., Didagelos, M., Ziakas, A., Didangelos, T., 2022. Insulin receptors and insulin action in the heart: the effects of left ventricular assist devices. Biomolecules. https://doi.org/10.3390/biom12040578.

Patterson, E., Walden, K.M., Khazaeli, M.B., Montgomery, D.G., Lucchesi, B.R., 1987. Changes in cardiac muscle function and biochemistry produced by long-term amiodarone and amiodarone + triiodothyronine administration in the Rabbit1. Pharmacology 35, 130–140.

Pessayre, D., Mansouri, A., Berson, A., Fromenty, B., 2010. Mitochondrial involvement in drug-induced liver injury. Handb. Exp. Pharmacol. 196, 311–365.

Poot, M., Zhang, Y.Z., Krämer, J.A., Wells, K.S., Jones, L.J., Hanzel, D.K., Lugade, A.G., Singer, V.L., Haugland, R.P., 1996. Analysis of mitochondrial morphology and function with novel fixable fluorescent stains. J. Histochem. Cytochem. 44, 1363–1372. https://doi.org/10.1177/44.12.8985128.

Rabkin, S.W., 2006. Effect of amiodarone on phospholipid content and composition in heart, lung, kidney and skeletal muscle: relationship to alteration of thyroid function. Pharmacology 76, 129–135. https://doi.org/10.1159/000090725.

Ramachandran, A., RGJ, V., Duan, L., Akakpo, J., Jaeschke, H., 2018. Mitochondrial dysfunction as a mechanism of drug-induced hepatotoxicity: current understanding and future perspectives. J. Clin. Transl. Res. 4, 75–100.

Reinhart, W.H., Rohner, F., 2023. Effect of amiodarone on erythrocyte shape and membrane properties. Clin. Sci. 79, 387–391.

Rieger, B., Krajčová, A., Duwe, P., Busch, K.B., 2019. ALCAT1 overexpression affects Supercomplex formation and increases ROS in respiring mitochondria. Oxidative Med. Cell. Longev. 2019 https://doi.org/10.1155/2019/9186469.

Rohani, L., Meng, G., Machiraju, P., Liu, S., Wu, J., Kovalchuk, I., Lewis, I., Shutt, T., Khan, A., Rancourt, D., Greenway, S., 2017. Modeling the dilated cardiomyopathy with ataxia syndrome (DCMA), a pediatric mitochondrial cardiomyopathy, using cardiomyocytes derived from induced pluripotent stem cells. Can. J. Cardiol. 33, S163–S164. https://doi.org/10.1016/j.cjca.2017.07.319.

Rosa, S.M.L.J., Antunes-Madeira, M.C., Jurado, A.S., Madeira, V.V.M.C., 2000. Amiodarone interactions with membrane lipids and with growth of *Bacillus stearothermophilus* used as a model. Appl. Biochem. Biotechnol. 87.

Sautereau, A.-M., Tournaire, C., Suares, M., Tocanne, J.-F., Pailloust, N., 1992. Interactions of amiodarone with model membranes and amiodarone-photoinduced peroxidation of lipids. Biochem. Pharmacol. 43, 2559–2566.

Silva Santos, L.F., Stolfo, A., Calloni, C., Salvador, M., 2017. Catechin and epicatechin reduce mitochondrial dysfunction and oxidative stress induced by amiodarone in human lung fibroblasts. J. Arrhythm. 33, 220–225.

Soar, J., Perkins, G.D., Maconochie, I., Böttiger, B.W., Deakin, C.D., Sandroni, C., Olasveengen, T.M., Wyllie, J., Greif, R., Lockey, A., Semeraro, F., van de Voorde, P., Lott, C., Bossaert, L., Monsieurs, K.G., Nolan, J.P., 2019. European resuscitation council guidelines for resuscitation: 2018 update – antiarrhythmic drugs for cardiac arrest. Resuscitation 134, 99–103. https://doi.org/10.1016/j.resuscitation.2018.11.018.

Spaniol, M., Bracher, R., Ha, H.R., Follath, F., Krähenbühl, S., 2001. Toxicity of amiodarone and amiodarone analogues on isolated rat liver mitochondria. J. Hepatol. 35, 628–636. https://doi.org/10.1016/S0168-8278(01)00189-1.

Steurer, G., Weber, H., Schmidinger, H., Plassi, H., Frey, B., Purerfellner, H., Probst, P., 1991. Plasma propafenone concentration in the evaluation of anti-arrhythmic efficacy. Eur. Heart J. 12, 526–532.

Stoschitzky, K., Stoschitzky, G., Lercher, P., Brussee, H., Lamprecht, G., Lindner, W., 2016. Propafenone shows class Ic and class II antiarrhythmic effects. Europace 18, 568–571. https://doi.org/10.1093/europace/euv195.

Tisdale, J.E., Chung, M.K., Campbell, K.B., Hammadah, M., Joglar, J.A., Leclerc, J., Rajagopalan, B., 2020. Drug-Induced Arrhythmias: A Scientific Statement from the American Heart Association. Circulation. https://doi.org/10.1161/CIR.0000000000000905.

Trohman, R., Sharma, P., McAninch, E., Bianco, A., 2019. Amiodarone and thyroid physiology, pathophysiology, diagnosis and management. Trends Cardiovasc. Med. 29, 285–295. https://doi.org/10.1016/j.tcm.2018.09.005.

Valembois, L., Audureau, E., Takeda, A., Jarzebowski, W., Belmin, J., Lafuente-Lafuente, C., 2019. Antiarrhythmics for maintaining sinus rhythm after cardioversion of atrial fibrillation. Cochrane Database Syst. Rev. https://doi.org/10.1002/14651858.CD005049.pub5.

Van Der Leij, F.R., Cox, K.B., Jackson, V.N., Huijkman, N.C.A., Bartelds, B., Kuipers, J.R. G., Dijkhuizen, T., Terpstra, P., Wood, P.A., Zammit, V.A., Price, N.T., 2002. Structural and functional genomics of the CPT1B gene for muscle-type carnitine palmitoyltransferase I in mammals. J. Biol. Chem. 277, 26994–27005. https://doi.org/10.1074/jbc.M203189200.

Varbiro, G., Toth, A., Tapodi, A., Veres, B., Sumegi, B., Gallyas, F., 2003. Concentration dependent mitochondrial effect of amiodarone. Biochem. Pharmacol. 65, 1115–1128. https://doi.org/10.1016/S0006-2952(02)01660-X.

Vater, M., Möckl, L., Gormanns, V., Schultz Fademrecht, C., Mallmann, A.M., Ziegart-Sadowska, K., Zaba, M., Frevert, M.L., Bräuchle, C., Holsboer, F., Rein, T., Schmidt, U., Kirmeier, T., 2017. New insights into the intracellular distribution pattern of cationic amphiphilic drugs. Sci. Rep. 7 https://doi.org/10.1038/srep44277.

Yim, W.W.Y., Mizushima, N., 2020. Lysosome biology in autophagy. Cell Discov. 6 https://doi.org/10.1038/s41421-020-0141-7.

Zeng, J., Shirihai, O.S., Grinstaff, M.W., 2020. Modulating lysosomal pH: a molecular and nanoscale materials design perspective. J. Life Sci. 2, 25–37. https://doi.org/10.36069/jols/20201204.

Zheng, W., Li, Y., Wang, Y., Yang, J., Zheng, C., Huang, X., Li, B., He, Q., 2017. Propafenone suppresses esophageal cancer proliferation through inducing mitochondrial dysfunction. Am. J. Cancer Res. 7, 2245–2256.